Cavity Ring-down Absorption Spectroscopy: Optical Characterization of ICl Product in Photodissociation of CH_2ICl at 248 nm

Denís Paredes-Roibás,[†] Muthiah Balaganesh,[‡,¶] Toshio Kasai,[‡,§] José María Gavira-Vallejo,[†] and King Chuen Lin[*,‡,¶]

†*Departamento de Ciencias y Técnicas Fisicoquímicas, Facultad de Ciencias, Universidad Nacional de Educación a Distancia (UNED), Paseo de la Senda del Rey 9, E-28040 Madrid, Spain*

‡*Department of Chemistry, National Taiwan Univeristy, Taipei 10617, Taiwan.*

¶*Institute of Atomic and Molecular Sciences, Academia Sinica, Taipei 10617, Taiwan.*

§*Institute of Scientific and Industrial Research, Osaka University, Ibaraki, Osaka 567-0047, Japan*

E-mail: kclin@ntu.edu.tw

Abstract

Iodine monochloride (ICl) elimination from one-photon dissociation of CH_2ICl at 248 nm is monitored by cavity ring-down absorption spectroscopy (CRDS). The spectrum of ICl is acquired in the transition of $B^3\Pi_0 \leftarrow X^1\Sigma^+$ and is confirmed to result from a primary photodissociation; that is, $CH_2ICl + h\nu \rightarrow CH_2 + ICl$. The vibrational population ratio is determined with the aid of spectral simulation to be 1:(0.36 ± 0.10):(0.11 ± 0.05) for the vibrational levels $v = 0$, 1 and 2 in the ground electronic state, corresponding to a Boltzmann-like vibrational temperature of 535 ± 69 K. The quantum yield of ICl molecular channel for the reaction is obtained to be 0.052 ± 0.026 using a relative method in which the scheme $CH_2Br_2 \rightarrow CH_2 + Br_2$ is adopted as the reference reaction. The ICl product contributed by the secondary collisions is minimized such that its quantum yield obtained is not overestimated. With the aid of CCSD(T)//B3LYP/MIDI! level of theory, the ICl elimination from CH_2ICl is evaluated to follow three pathways via either (1) a three-center transition state or (2) two isomerization transition states. But the three-center concerted mechanism is verified to be unfavorable.

Abbreviations

CRDS, PES, RRKM, DFT

1 Introduction

Polyhalomethanes like CH_2I_2, CH_2Br_2, $CHBr_3$, CH_2BrI, CH_2ClI, and $CHBr_2Cl$ are probably the main sources of reactive halogens (X) in the atmosphere. The subsequent reactions of reactive halogens with O_3 to form XO radical initiate various tropospheric ozone depleting cycles.[1] Apart from ozone depletion, especially iodine plays a significant role in the formation of marine aerosol and cloud condensation nuclei, thus affecting the climate.[2] The main sources of polyhalomethanes are algae and phytop-lankton present in ocean. Though these compounds dissolve in the oceanic water and marine boundary layer, measurable quantities of gases escape into the atmosphere.[3] Among the polyhalomethanes, CH_2ICl is one of the important and interesting compounds which contains both iodine and chlorine. For instance, various measurements[4–6] have shown seawater concentrations of CH_2ICl in the northwestern Atlantic to be comparable to or greater than that of CH_3I. Also it is reported that CH_2ICl is the potential source for atmospheric iodine compared to CH_3I. By solar irradiation, the CH_2ICl can be photo-dissociated to various products (CH_2, CH_2I, CH_2Cl, CHCl, CHI, I, I*, Cl, Cl*, HI, HCl and ICl); such photo-dissociation may proceed both in solution and in the atmosphere.[2] In this study, the photodissociation of CH_2ICl was focused on the production of ICl; this channel is optically characterized for the first time.

Various previous works have been dedicated to the studies of the photo-dissociation of CH_2ICl in gas phase. For example, Senapati et al.[7,8] used resonance-enhanced multiphoton ionization (REMPI) technique to study photo dissociation of CH_2ICl at different excitation wavelengths (222, 266, 280, and ∼304 nm). They measured the quantum yield for the production of I*($^2P_{1/2}$) and Cl*($^2P_{1/2}$) corresponding to the transitions from $^3Q_0$(C-I) and $^1Q_1$(C-I) states[7] and from the $^3Q_0$(C-Cl) state,[8] respectively. The quantum yields of I* and Cl* obtained lie in between 0.22 and 0.55 at various photolysis wavelengths; among them, I* yields a larger value for each wavelength.[7,8]

Tu et al.[9] used laser-induced fluorescence (LIF) technique to study the photolysis of different polyhalomethanes such as CHI_3, CH_2I_2, CH_3I, and CH_2ICl at 266 nm in a slow flow

cell at ambient temperature. Among the emission spectra of CH, C_2 and I_2 observed, they reported that most of the observed I_2 molecules result from the collisional product between the atomic iodine from photodissociation, instead of any molecular elimination channels.

Schmitt et al.[10] studied the photo decomposition of CH_2ICl at 266 nm using gas chromatographic technique to analyze carbon containing products. They have identified eight products (C_2H_3Cl, C_2H_4, C_2H_2, $C_2H_4Cl_2$, trans-$C_2H_2Cl_2$, CH_2Cl_2, cis-$C_2H_2Cl_2$ and I_2) which are formed mostly from secondary and recombination reactions. But they could not detect the primary photodissociation products such as HCl, HI and ICl. Other pathways were explored by Zhang et al.[11] using laser photo-fragmentation time-of-flight mass spectrometric method at 193 nm. They obtained the kinetic energy distributions for the predominant products such as $I(^2P_{1/2})$, $I(^2P_{3/2})$, $Cl(^2P_{1/2,3/2})$, singlet HCl and singlet ICl, and evaluated the branching ratio for the formation of $I(^2P_{1/2})$ and $I(^2P_{3/2})$. In addition, they theoretically predicted the production mechanism to CH_2 + ICl through an isomerization transition state. With an alternative technique of time-resolved electronic absorption spectroscopy, Preston et al.[12] probed the isomerization of CH_2ICl into iso-CH_2-Cl-I, which turned out to proceed in a high excited level with a brief lifetime prior to photo-dissociation.

Šulkova et al.[13] studied theoretically the reaction of OH radicals with CH_2ICl, showing the atmospheric lifetime for the CH_2ICl removal is about 1 year. They thus concluded that the atmospheric loss of CH_2ICl due to the oxidation by OH radicals is not as rapid as with the oxidation by Cl atoms and photodissociation of CH_2ICl by UV light.

Apart from the gas-phase reaction, a few studies were reported in photoexcitation of several polyhalomethanes including CH_2ICl in dilute solutions using femtosecond transient absorption and time-resolved resonance Raman spectroscopy.[14–18] Åkesson and co-workers[14] reported the femtosecond transient absorption on the photolysis of CH_2ICl in acetonitrile solution at room temperature. They observed iso-CH_2Cl-I as first photoproduct with life time 100 ps and then ICl^- as the second photoproduct at longer times. Philips group[15] investigated the initial formation and subsequent decay of the photoproduct produced following 267

nm excitation of CH_2ICl in acetonitrile solution. They suggested that the iso-CH_2Cl-I photoproduct is first produced from initially formed CH_2ICl and I fragments via recombination within the solvent cage, followed by isomerization to give either the more stable iso-CH_2Cl-I or parent CH_2ICl molecules.

This work aims to study the ICl production channel using cavity ring-down absorption spectroscopy (CRDS) at 248 nm. A detailed characterization of this molecular pathway will be reported, such as (i) acquisition of ro-vibrational spectra of the ICl fragment in the $B^3\Pi_0 \leftarrow X^1\Sigma^+$ transition, accompanied by the corresponding spectral simulation, (ii) determination of vibrational branching ratios of ICl (v"=0, 1, and 2) and the quantum yield for the ICl molecular channel, (iii) verification of ICl formation resulting from primary one-photon dissociation of CH_2ICl (i.e., $CH_2ICl + h\nu \rightarrow CH_2 + ICl$), instead of a secondary reaction (e.g., $I + CH_2ICl \rightarrow CH_2I + ICl$), and (iv) ab initio calculations of dissociation pathways for the ICl channel, followed by evaluation of the Rice-Ramsperger-Kassel-Marcus[19,20] (RRKM) rate constants. Finally, the ICl production process is compared with Br_2, and I_2 elimination from CH_2Br_2 and CH_2I_2, respectively.

2 Experimental setup

The experimental setup of the CRDS apparatus has been described elsewhere[21–27] In brief, the CRDS is composed of three units, a ring-down flow cell, the photolysis-and-probe laser system and the ring-down time detection and signal analysis.A KrF excimer laser,emitting at 248 nm with the energy 10-30 mJ/pulse, was employed for photolysis.An Nd:YAG-pumped dye laser, operating with the dyes of sulforhodamine B (588-614 nm) or coumarin 503 (485-546 nm), was used as the ICl probe beam with the energy regulated about 2-4 mJ. The beam was guided through a spatial filter to select the TEM_{00} mode.

Two sets of highly reflective mirrors were mounted to the long-arms of a cross-shaped stainless steel cavity, one for the 485-546 nm range and the other for the 588-614 nm range.

Both sets of mirrors have a reflectivity of 99.95% with 1 m radius of curvature and a diameter of 25.4 mm. The photolysis beam, focused via a 25-cm focal-length cylindrical lens, propagated through the short-arms to overlap with the CRDS probe beam perpendicularly. The ring-down time was monitored by a photo-multiplier tube sitting behind the rear mirror. To avoid pollution by chemical contact with the mirrors,an argon gas was kept to flow constantly across the cavity. Prior to introduction of the reagents, CH_2ICl (Acros) and the ICl (Acros), a freeze-pump-thaw system at 77K was used up to 3-4 times. The absorption coefficient α and the subsequent concentration of ICl may be determined by the fit of the acquired ring-down time (τ), according to the equation (1)

$$\alpha(\lambda) = \frac{d}{cl}\left[\frac{1}{\tau} - \frac{1}{\tau_0}\right] \tag{1}$$

where d is the length of cavity, l is the length of light interacting with samples, c is the velocity of light, and τ and τ_0 denote the ring-down time with and without the sample present in the ring-down cell, respectively. The ICl absorption spectra was recorded with a spectral resolution of 0.1 cm^{-1}. The signal was acquired and analyzed with the aid of a MATLAB laboratory-developed software.

3 Theoretical methods

We characterized the adiabatic singlet ground-state potential energy surface (PES) of the various dissociation channels of CH_2ICl dissociation. The geometries of the species involved (reactant, transition states and products) in the CH_2ICl dissociation were optimized using hybrid density B3LYP[28,29]/MIDI![30,31] functional theory. Harmonic frequencies and the zero point energies of all the species were obtained using the same level of theory. Both reactant and products were obtained with all positive frequencies and the transition state with one imaginary frequency. We further performed the intrinsic reaction coordinate (IRC) using the Gonzalez and Schlegel[32,33] second-order algorithm to verify the connections between the

transition state and the reactant and products. Finally, we employed the CCSD(T)/MIDI! method on optimized geometries to get a more accurate energy. The basis set MIDI! was utilized for its moderate size for the heavy atom I, and succeeded in predicting a reasonable ICl bond length. These calculations were carried out using the Gausian09 suite of program.[34] The RRKM rate constant was calculated for the formation of ICl from photo-dissociation of ground state of CH_2ICl at 248nm.

4 Results and Discussion

4.1 Rovibrational spectra of ICl fragment

Using CRDS, we acquired the ro-vibrational spectra of ICl (v" = 0, 1 and 2) from 591 to 606 nm in the $B^3\Pi_0 \leftarrow X^1\Sigma^+$ transition produced by the photo-dissociation of the CH_2ICl at 248 nm. Fig. 1 shows a portion of the CRDS spectrum of the ICl fragment, accompanied by the pure ICl spectrum in the same region. The agreement between the spectra is reasonably good and leads to the conclusion that ICl is produced from the CH_2ICl photo-dissociation and the spectral region is not interfered by other fragmented species.

To check if there are any secondary reactions which contributed to ICl, we compare with the pure I_2 spectrum recorded under otherwise the same conditions. As shown in Fig. 2, no significant trace of I_2 is found in the ICl spectrum. As a result, one can conclude that the ICl fragment is eliminated by the primary photo-dissociation of CH_2ICl and its contribution by the secondary reaction should be negligible. If the secondary reaction does happen, one might observe formation of either product of ICl, Cl_2 and I_2 according to the following

secondary reactions (2a-2f).

$$I + CH_2ClI \rightarrow I_2/ICl + \text{other fragments} \quad (2a)$$

$$I + CH_2Cl \rightarrow ICl + \text{other fragments} \quad (2b)$$

$$I + CH_2I \rightarrow I_2 + \text{other fragments} \quad (2c)$$

$$Cl + CH_2ICl \rightarrow Cl_2/ICl + \text{other fragments} \quad (2d)$$

$$Cl + CH_2Cl \rightarrow Cl_2 + \text{other fragments} \quad (2e)$$

$$Cl + CH_2I \rightarrow ICl + \text{other fragments} \quad (2f)$$

Among the above products, a larger amount of I_2 is expected in the secondary reactions, and a larger quantum yield of I* with respect to Cl* was also detected in the photolysis at varied wavelengths,[7,8] because the C-I bond energy is smaller than the C-Cl bond energy. In addition, the experimental condition of CH_2ICl at 34 mTorr (Fig. 5) corresponds to a concentration of 1.2×10^{15} molecules/cm^3. The I atomic elimination should be the major channel, which is assumed to take a yield of 50 %, corresponding to 6×10^{14} molecules/cm^3. Given a relative speed 3×10^4 cm/s at 300 K between CH_2ICl and I and the collision cross section of 35 Å^2, each CH_2ICl molecule may encounter ~0.3 collisions by the released I during the ring-down time of 5 μs. Thus, the ICl product resulting from the secondary collision (i.e., I + CH_2ICl→ ICl + CH_2I) is negligible. The calculated result is consistent with the experimental finding. In addition, the root-mean-squared distance that the ICl molecules diffuse within a detection period of 4-5 μs ring-down time is about 1 mm, which is confined within the cross section (diameter = 3 mm) along the detection axis and within the photolysis-probe delay time of 20 ns.

To find out how many photon number are involved in the photolysis, rotational line intensity of ICl spectrum at 519.685 nm was measured as a function of the photolysis laser energy. As shown in Fig. 3b, the resulting plot yields a straight line which supports the

single-photon involvement in the molecular elimination of ICl. In addition to the above measurements, the CH_2ICl pressure dependence of the ICl product was conducted. Given a constant photolysis laser energy, the plot of the ICl concentration as a function of the CH_2ICl pressure (0.1 -2 Torr) yields a straight line, as shown in Fig 4. Because the channel of halogen atomic elimination dominates over the dissociation pathways, the pseudo-first order reaction cannot be applied to the secondary reactions (2a-2f). Thus, the ICl product contributed from the reaction of a halogen atom with precursor requires two CH_2ICl molecules involved. The result lends the support to the fact that the ICl contribution from the secondary reactions should be minimal.

The CRDS spectral regions were carefully selected to contain the v" = 0, 1 and 2 bands. For instance, the ICl spectrum in the 595.80-596.60 nm region contains the vibrational bands (v', v") = (14,0) and (13,1) of the $B^3\Pi_0 \leftarrow X^1\Sigma^+$ transition. Similarly, the spectrum in the region of 598.0-598.4 nm corresponds to the bands of (v', v") = (14,0), (16,1) and (1,2). Fig.5 displays the ICl fragment in the 598.0-598.4 nm region, in wich we also include the pure ICl spectrum and the simulated counterpart for individual vibrational band with appropriate adjustment of the population ratio of ICl(v"=1)/ICl(v"=0) and ICl(v"=2)/ICl(v"=1). When ICl(v"=1)/ICl(v"=0) is fixed at 0.36 and ICl(v"=2)/ICl(v"=1) is adjusted to 0.11, the spectral simulation becomes appreciably consistent with the experimental finding.

Given the same population ratio for ICl (v"=0,1, and 2), Fig. 6 shows comparison of ICl fragment with the simulated counterpart in the region of 605-605.8 nm which contains the (v',v") bands of (14,0), (13,1), (14,1), (0,2) and (2,3). The population of v"=3 is buried seriously in those populations of v"=0, 1, and 2 and thus can not be evaluated accurately.

4.2 Simulation and rotational populations

Despite a long ring-down time averaged to 5 μs, the vibrational population may be preserved approximately in the nascent state for the vibrational energy transfer is slow, but the rotational population is rapidly thermally equilibrated. The reported Franck-Condon factors

(FCFs) are available in the literature only for a few transitions.[35,36] Thus, it is required to calculate the potential energy curves involved in the transition and subsequently evaluate the FCFs for simulation of the ICl spectra. To construct these potential energy curves, the spectroscopic parameters of $B^3\Pi_0$ and $X^1\Sigma^+$ electronic states are obtained from the previous work.[37] Then, the potential energy curves for the $B^3\Pi_0$ and $X^1\Sigma^+$ electronic states of ICl can be calculated using Rydberg[38,39]-Klein[40]-Rees[41] (RKR) method.[42] The FCFs was evaluated as the extent of overlap integral between the vibrational wavefunctions of the $B^3\Pi_0$ and $X^1\Sigma^+$ electronic states with the aid of LEVEL program.[43] Given FCFs obtained (see Supporting Information, SI), then the spectral intensities of ICl spectrum can be calculated using the equation (3)[44]

$$I = k\frac{(FCF)(HLF)}{2J" + 1}N_{J"}r_{iso}f \tag{3}$$

where k is a factor associated with instrument and experimental conditions, FCF the Franck-Condon factors, HLF the Hönl-London-London factor, $J"$ the rotational quantum number of the ground state ICl, $N_{J"}$ the Boltzmann distribution of the rotational population for which 300 K is assumed, r_{iso} the ratio of isotopic variants, $I^{35}Cl$:$I^{37}Cl$ equal to 0.7576 : 0.2424, and f the intensity ratio of strong and weak rotational lines.

The molecular constants of ground ($X^1\Sigma^+$) and excited ($B^3\Pi_0$) states of $I^{35}Cl$ used in the present study are given in Table 1. As for $I^{37}Cl$, its molecular constants were derived by applying isotopic effect.

Table 1: molecular constants (cm^{-1}) of ground ($X^1\Sigma^+$) and excited ($B^3\Pi_0$) states of $I^{35}Cl$.

Electronic state	$w_e(cm^{-1})$	$w_ex_e(cm^{-1})$	$w_ey_e(cm^{-1})$	$D_e(cm^{-1})$	$B_e(cm^{-1})$
$X^1\Sigma^+$	384.293	1.501		4.03×10^{-8}	0.0872
$B^3\Pi_0$	204.5	2.595	-0.937	1.00×10^{-7}	0.0872

To estimate the uncertainty for the simulation, a comparison between the experimental spectra and the simulation evaluated for different population ratios in the regions of 596.50-596.55 nm and 598.09-598.12 nm is shown in the Fig. 7. A population ratio ICl($v" =$

0)/ICl(v" = 1) is then optimized to be 0.36 ± 0.10 in the range of 596.50-596.55 nm. Given ICl(v" = 0)/ICl(v" = 1) fixed at 0.36, the ICl(v" = 0)/ICl(v" = 2) ratio in the 598.09-598.12 range can be optimally adjusted to 0.11 ± 0.05. Accordingly, the population ratio of v" = 0:1:2 is equal to 1:(0.36 ± 0.10):(0.11 ± 0.05) corresponding to the Boltzmann vibrational temperature 535 ± 69 K .

4.3 Quantum yield for ICl channel

The quantum yield for the formation of ICl from the CH_2ICl photo-dissociation is evaluated by [ICl]/N_p, in wich [ICl] denotes the ICl concentration produced in the laser beam-crossed region and N_p the number density of photon absorbed in the same region. Alternatively, the quantum yield for the ICl channel can be determined by the indirect method, when the quantum yields of similar reactions are well established.The Br_2 formation from CH_2Br_2 photo-dissociation studied in a previous work was chosen as reference reaction with the quantum yield of 0.21 ± 0.06[21,27] The following equation is used to calculate the quantum yield of ICl production

$$\frac{\Phi_{\mathrm{ICl}}}{\Phi_{\mathrm{Br_2}}} = \frac{[ICl]n_{\mathrm{CH_2Br_2}}\sigma_{\mathrm{CH_2Br_2}}}{[\mathrm{Br_2}]n_{\mathrm{CH_2ICl}}\sigma_{\mathrm{CH_2ICl}}} \tag{4}$$

where [ICl] and [Br_2] are concentrations obtained from the experiment, $n_{\mathrm{CH_2ICl}}$ and $n_{\mathrm{CH_2Br_2}}$ the number density of CH_2ICl and CH_2Br_2, $\sigma_{\mathrm{CH_2ICl}}$ and $\sigma_{\mathrm{CH_2Br_2}}$ are the absorption cross sections of CH_2ICl and CH_2Br_2 at 248 nm. We evaluated Br_2 concentration to be 8.1 $\times 10^{15}$ molecules/cm^3 at the rotational line of 519.68 nm by the ring-down time measurements, and $n_{\mathrm{CH_2Br_2}}$ was experimentally controlled to 596 mTorr. By analogy, the ICl concentration was evaluated to be 4.7 $\times 10^{14}$ molecules/cm^3 at the almost identical rotational line, and $n_{\mathrm{CH_2ICl}}$ was controlled at 300 mTorr. Given $\sigma_{\mathrm{CH_2Br_2}}$ evaluated to be 3.7 $\times 10^{-19}$ cm^2, $\sigma_{\mathrm{CH_2ICl}}$ equal to 1.52 $\times 10^{-19}$ cm^2 and the Br_2 quantum yield of 0.2 ± 0.06, substituting the above values into the equation yields a quantum yield of 0.052 ± 0.026 for ICl elimination

from CH_2ICl photolysis. The uncertainty in the quantum yield value was estimated using error propagation formula as given in equation 5.

$$\Delta\phi_{ICl} = \phi_{ICl}\sqrt{\left(\frac{\Delta[ICl]}{[ICl]}\right)^2 + \left(\frac{\Delta[Br_2]}{[Br_2]}\right)^2 + \left(\frac{\Delta\sigma_{CH_2Br_2}}{\sigma_{CH_2Br_2}}\right)^2 + \left(\frac{\Delta\sigma_{CH_2ICl}}{\sigma_{CH_2ICl}}\right)^2 + \left(\frac{\Delta n_{CH_2Br_2}}{n_{CH_2Br_2}}\right)^2 + \left(\frac{\Delta n_{CH_2ICl}}{n_{CH_2ICl}}\right)^2 + \left(\frac{\Delta\phi_{Br_2}}{\phi_{Br_2}}\right)^2} \quad (5)$$

In comparison with this result, the quantum yields of Br_2 and I_2 produced from photodissociation of CH_2Br_2,[23,27] and CH_2I_2,[26] at the same wavelength yielded the values of 0.21 $\pm$ 0.06 and 0.004 $\pm$ 0.0025 respectively. The quantum yield for the ICl channel from CH_2ICl is smaller by a factor of four than that of Br_2 from CH_2Br_2, but ten times larger than I_2 from CH_2I_2. The obtained order of quantum yields of Br_2, ICl and I_2 apparently does not follow the strength of the C-X bond rupture. It is impossible to interpret the trend without taking into account the branching ratios of X elimination in the excited and ground state of halo-carbons and the efficiency of internal conversion from the state $B^3\Pi_0$ to $X^1\Sigma^+$.

4.4 Photodissociation mechanism

The density functional theory was applied to study the photo dissociation mechanism of the CH_2ICl molecule. The analysis of the PES was carried out and the geometries for reactant (CH_2ICl), the transition states (tsICl, tsCH_2-I-Cl, tsCH_2-Cl-I, tsCHI and ts CHCl) and products (CH_2, ICl, CH_2-I-Cl, HI, HCl, CHI and CHCl) were optimized by the aid of the B3LYP/MIDI! level of theory. The calculations lead to a result of no negative frequencies for the CH_2ICl, CH_2, ICl, CH_2-I-Cl, HI, HCl, CHI and CHCl, but a negative frequency for all transition states. To confirm that the transition states are connected with the reactant and the products, IRC calculations were conducted on all the transition states for the different reactions paths.

The high level CCSD(T) calculations were further carried out on the B3LYP optimized ge-

ometry to obtain more accurate energy. The B3LYP/MIDI! zero-point and CCSD(T)/MIDI! energies of all geometries are tabulated in S.I. The optimized geometries for the three-center elimination path and the two possible isomerization paths are displayed in Fig. 8 with internal coordinates. As shown in the figure the bond distances for the C-I, C-Cl in the reactant are up to 1.802 Å and 2.188 Å respectively. In contrast, the corresponding bond distances are elongated to 2.273 Å and 3.005 Å in the transition state tsCH_2ICl. In the case of the ICl product, the equilibrium bond length of Cl-I is 2.336 Å while the corresponding distance in the transition state is about 2.430 Å. The bond angle of I-C-Cl is shortened to 68.5° in the tsCH_2ICl from 114° in the reactant.

The ground state CH_2ICl decomposes into CH_2 and ICl via tsCH_2ICl with a barrier height of 437 kJ/mol. The reaction scheme is endothermic with the energy of 436 kJ/mol. The dissociation pathways for the CH_2ICl to form ICl were evaluated by the theory of CCSD(T)//B3LYP/MIDI! level and shown in Fig. 9.

In addition to PES exploration, density and sum of states were calculated for reactant and transition states using Baeyer-swineheart algorithm implemented in multiwell program.[45,46] The unimolecular rate constants for the dissociation channel ($CH_2ICl \rightarrow CH_2 + ICl$) were then calculated using equation (6).

$$k(E) = \frac{1}{h}\frac{G(E)}{N(E - E_r)} \tag{6}$$

where h is the Planck's constant, $G(E)$ is the sum of states for the active degrees of freedom at the transition state and $N(E - E_r)$ is the vibrational density of states for the active degrees of freedom in the reactanct. The calculated sum of vibrational states for the different path's transition states as a function of the excitation energy are shown in Fig. S1. Also the density of states for the reactant (CH_2ICl) as a function of the excitation energy are shown in Fig. S2. Comparison of the rate constants between three-center elimination and the isomerization pathway is given in Table 2. Despite much larger rates to surpass

the isomerization transition states (k_2 and k_3 paths), the net rates are impeded by the endothermicity. Similar pathway with isomerization transition state is also found in the elimination of I_2 from CH_2I_2.[28]

Zhang et al.[11] have calculated the dissociation pathway in which the ICl(singlet state) + CH_2(singlet state) were produced only via an isomerization transition state, Cl sitting in between C and I (the k_3 path). In contrast, we find out three reaction mechanisms, one with three-center concerted elimination and the other two surpassing isomerization transition state (k_2 and k_3 paths in Fig. 9). Despite the photolysis energy higher than the barrier along the k_1 path, the three-center concerted elimination should result in a triplet CH_2 and triplet ICl for electron-spin conservation. The ground triplet state CH_2 has been verified unfavorable in kinetic energy analysis of the CH_2 + ICl channel.[11] In addition, the ICl fragment detected with CRDS is confirmed to lie in the singlet ground state. Thus, it is difficult for the CH_2ICl molecule to follow the k_1 path leading to the ICl fragment. Apart from the k_3 path reported previously by Zhang et al., we find herein that the k_2 path proceeding via an isomerization transition state with I sitting in between C and Cl is available to produce the CH_2 + ICl channel.

In the gas reaction, ICH_2Cl proceeds to CH_2 + ICl via an isomerization transition state of CH_2I–Cl or CH_2Cl–I with the barrier of 352 or 282 kJ/mol, respectively. In contrast, the isomerization step CH_2I–Cl with a much lower energy barrier of 167 kJ/mol was also found in the solution phase via a recombination between CHI and Cl by the solvent cage effect. Despite the same isomerization step, the reaction mechanism between gas and liquid phases turn out to be different.

Table 2: Rate constants comparison between different paths.

Reactions	Rate constants (s^{-1}) at 248 nm
$CH_2ICl \rightarrow CH_2$ + ICl	$k_1 = 1.026 \times 10^8$
$CH_2ICl \rightarrow CH_2$-I-Cl	$k_2 = 1.451 \times 10^{10}$
$CH_2ICl \rightarrow CH_2$-Cl-I	$k_3 = 1.637 \times 10^{11}$

5 Conclusions

The ICl fragment elimination from the photolysis of CH_2ICl at 248nm was demonstrated by using the CRDS technique. The acquired ICl (v"=0, 1, and 2) spectra in the $B^3\Pi_0 \leftarrow X^1\Sigma^+$ transition are simulated to obtain the vibrational population ratio and the corresponding Boltzmann vibrational temperature. The quantum yield of the ICl channel was estimated. Its value lies in between the Br_2 and I_2 elimination from CH_2Br_2 and CH_2I_2, respectively. However, interpretation for the trend of the quantum yields cannot simply rely on the strength of the C-X bond rupture. We also verify that the ICl fragment should result from the reaction, $CH_2ICl + h\nu \rightarrow CH_2 + ICl$, involving one-photon mechanism, and the ICl contribution from secondary reactions is negligible. With the aid of theoretical calculations, three dissociation pathways are calculated. The ICl product can be formed via either a three-center concerted transition state or two isomerization transition states. While taking into account the electron-spin conservation, the latter path following isomerization mechanism is favored.

6 Supporting Information

The Franck-Condon factors correspond to the ground ($X^1\Sigma^+$) and excited ($B^3\Pi_0$) states, sum and density of states correspond to optimized reactant and transition states, Energies of various species involved in the photo-dissociation of CH_2ICl obtained at B3LYP and CCSD(T) level of theories.

Acknowledgement

This work is supported by Ministry of Science and Technology of Taiwan, Republic of China under Contract No. NSC 102-2113-M-002-009-MY3 and the ERASMUS MUNDUS EURASIACAT project (Advanced Education European-Asiatic Exchange Programme in Materials Science and Catalysis, with ref. nr. 552067). Computer resources at the National Center

for High-performance Computer of Taiwan were utilized in the calculations.

References

1. Murillo-Sánchez, M.; Poullain, S. M.; González-Vázquez, J.; Corrales, M.; Balerdi, G.; Bañares, L. Femtosecond photodissociation dynamics of chloroiodomethane in the first absorption band. *Chem. Phys. Lett.* **2017**, *683*, 22–28.

2. Jones, C. E.; Carpenter, L. J. Solar photolysis of CH_2I_2, CH_2ICl, and CH_2IBr in water, saltwater, and seawater. *Environ. Sci. Technol.* **2005**, *39*, 6130–6137.

3. Vogt, R.; Sander, R.; Von Glasow, R.; Crutzen, P. J. Iodine chemistry and its role in halogen activation and ozone loss in the marine boundary layer: A model study. *J. Atmos. Chem.* **1999**, *32*, 375–395.

4. Class, T.; Kohnle, R.; Ballschmiter, K. Chemistry of organic traces in air VII: bromo-and bromochloromethanes in air over the Atlantic Ocean. *Chemosphere* **1986**, *15*, 429–436.

5. Class, T.; Ballschmiter, K. Chemistry of organic traces in air. *J.Atmos. Chem.* **1988**, *6*, 35–46.

6. Moore, R. M.; Tokarczyk, R. Chloro-iodomethane in N. Atlantic waters: A potentially significant source of atmospheric iodine. *Geophys. res. lett.* **1992**, *19*, 1779–1782.

7. Senapati, D.; Kavita, K.; Das, P. K. Photodissociation Dynamics of CH_2ICl at 222, 236, 266, 280, and 304 nm. *J. Phys. Chem. A* **2002**, *106*, 8479–8482.

8. Senapati, D.; Das, P. K. $Cl^*(^2P_{1/2})$ production dynamics from chloroiodomethane (CH_2ICl) in the ultraviolet. *Chem. Phys. Lett.* **2004**, *393*, 535–538.

9. Tu, C.-P.; Cheng, H.-I.; Chang, B.-C. Spectroscopic Study of the I_2 Formation from the Photolysis of Iodomethanes (CHI_3, CH_2I_2, CH_3I, and CH_2ICl) at Different Wavelengths. *J. Phys. Chem. A* **2013**, *117*, 13572–13577.

10. Schmitt, G.; Comes, F. Competitive photodecomposition reactions of chloroiodomethane. *J. Photochem. Photobiol. A* **1987**, *41*, 13–30.

11. Zhang, T.; Ng, C.; Qi, F.; Lam, C.-S.; Li, W.-K. A 193 nm laser photofragmentation time-of-flight mass spectrometric study of chloroiodomethane. *J. Chem. Phys.* **2005**, *123*, 174316.

12. Preston, T. J.; Dutta, M.; Esselman, B. J.; Kalume, A.; George, L.; McMahon, R. J.; Reid, S. A.; Fleming Crim, F. Formation and relaxation dynamics of iso-CH_2Cl–I in cryogenic matrices. *J. Chem. Phys.* **2011**, *135*, 114503.

13. Šulková, K.; Šulka, M.; Louis, F.; Neogrády, P. Atmospheric Reactivity of CH_2ICl with OH Radicals: High-Level OVOS CCSD (T) Calculations for the X-Abstraction Pathways (X= H, Cl, or I). *J. Phys. Chem. A* **2013**, *117*, 771–782.

14. Tarnovsky, A. N.; Wall, M.; Rasmusson, M.; Pascher, T.; Åkesson, E. Photodissociation Dynamics of Chloroiodomethane in Acetonitrile Studied by Ultrafast Pump-Probe Spectroscopy. *J. Chin. Chem. Soc.* **2000**, *47*, 769–772.

15. Kwok, W. M.; Ma, C.; Parker, A. W.; Phillips, D.; Towrie, M.; Matousek, P.; Zheng, X.; Phillips, D. L. Picosecond time-resolved resonance Raman observation of the iso-CH_2Cl–I and iso-CH_2I–Cl photoproducts from the "photoisomerization" reactions of CH_2ICl in the solution phase. *J. Chem. Phys.* **2001**, *114*, 7536–7543.

16. Zheng, X.; Phillips, D. L. Photoisomerization reaction of CH_2BrI following A-band and B-band photoexcitation in the solution phase: Transient resonance Raman observation of the iso-CH_2I–Br photoproduct. *J. Chem. Phys.* **2000**, *113*, 3194–3203.

17. Kwok, W. M.; Ma, C.; Parker, A. W.; Phillips, D.; Towrie, M.; Matousek, P.; Phillips, D. L. Picosecond time-resolved resonance Raman observation of the iso-CH_2I–I photoproduct from the "photoisomerization" reaction of diiodomethane in the solution phase. *J. Chem. Phys.* **2000**, *113*, 7471–7478.

18. Zheng, X.; Phillips, D. L. Solvation can open the photoisomerization pathway for the direct photodissociation reaction of diiodomethane: Transient resonance raman observation of the isodiiodomethane photoproduct from ultraviolet excitation of diiodomethane in the solution phase. *J. Phys. Chem. A* **2000**, *104*, 6880–6886.

19. Chang, A. H.; Mebel, A.; Yang, X.-M.; Lin, S.; Lee, Y. Ab initio/RRKM approach toward the understanding of ethylene photodissociation. *J. Chem. Phys.* **1998**, *109*, 2748–2761.

20. Chang, A.; Hwang, D.; Yang, X.-M.; Mebel, A.; Lin, S.; Lee, Y. Toward the understanding of ethylene photodissociation: Theoretical study of energy partition in products and rate constants. *J. Chem. Phys.* **1999**, *110*, 10810–10820.

21. Wu, C.-C.; Lin, H.-C.; Chang, Y.-B.; Tsai, P.-Y.; Yeh, Y.-Y.; Fan, H.; Lin, K.-C.; Francisco, J. Br_2 molecular elimination in photolysis of $(COBr)_2$ at 248 nm by using cavity ring-down absorption spectroscopy: A photodissociation channel being ignored. *J. Chem. Phys.* **2011**, *135*, 234308.

22. Huang, H. Y.; Chuang, W. T.; Sharma, R. C.; Hsu, C. Y.; Lin, K. C.; Hu, C. H. Molecular elimination of Br_2 in 248 nm photolysis of bromoform probed by using cavity ring-down absorption spectroscopy. *J. Chem. Phys.* **2004**, *121*, 5253–60.

23. Wei, P.-Y.; Chang, Y.-P.; Lee, W.-B.; Hu, Z.; Huang, H.-Y.; Lin, K.-C.; Chen, K.; Chang, A. 248 nm photolysis of CH_2Br_2 by using cavity ring-down absorption spectroscopy: Br_2 molecular elimination at room temperature. *J. Chem. Phys.* **2006**, *125*, 133319.

24. Wei, P.-Y.; Chang, Y.-P.; Lee, Y.-S.; Lee, W.-B.; Lin, K.-C.; Chen, K.; Chang, A. B_2 molecular elimination in 248 nm photolysis of $CHBr_2Cl$ by using cavity ring-down absorption spectroscopy. *J. Chem. Phys.* **2007**, *126*, 034311.

25. Hsu, C. Y.; Huang, H. Y.; Lin, K. C. Br_2 elimination in 248-nm photolysis of CF_2Br_2 probed by using cavity ring-down absorption spectroscopy. *J. Chem. Phys.* **2005**, *123*, 134312.

26. Chen, S.-Y.; Tsai, P.-Y.; Lin, H.-C.; Wu, C.-C.; Lin, K.-C.; Sun, B.; Chang, A. I_2 molecular elimination in single-photon dissociation of CH_2I_2 at 248 nm by using cavity ring-down absorption spectroscopy. *J. Chem. Phys.* **2011**, *134*, 034315.

27. Chen, B.-J.; Tsai, P.-Y.; Huang, T.-K.; Xia, Z.-H.; Lin, K.-C.; Chiou, C.-J.; Sun, B.-J.; Chang, A. Characterization of molecular channel in photodissociation of $SOCl_2$ at 248 nm: Cl_2 probing by cavity ring-down absorption spectroscopy. *Phys. Chem. Chem. Phys.* **2015**, *17*, 7838–7847.

28. Becke, A. Density-functional thermochemistry. III. The role of exact exchange. *J. Chem. Phys.* **1993**, *98*, 5648.

29. Lee, C.; Yang, W.; Parr, R. G. Development of the Colle-Salvetti correlation-energy formula into a functional of the electron density. *Phys. Rev. B.* **1988**, *37*, 785–789.

30. Feller, D. The role of databases in support of computational chemistry calculations. *J. Comput. Chem.* **1996**, *17*, 1571–1586.

31. Schuchardt, K. L.; Didier, B. T.; Elsethagen, T.; Sun, L.; Gurumoorthi, V.; Chase, J.; Li, J.; Windus, T. L. Basis set exchange: a community database for computational sciences. *J. Chem. Inf. Model.* **2007**, *47*, 1045–1052.

32. Gonzalez, C.; Schlegel, H. B. An Improved Algorithm for Reaction-Path Following. *J. Chem. Phys.* **1989**, *90*, 2154–2161.

33. Gonzalez, C.; Schlegel, H. B. Reaction path following in mass-weighted internal coordinates. *J. Phys. Chem.* **1990**, *94*, 5523–5527.

34. Frisch, M.; Trucks, G.; Schlegel, H. B.; Scuseria, G.; Robb, M.; Cheeseman, J.; Scalmani, G.; Barone, V.; Mennucci, B.; Petersson, G. Gaussian 09, revision a. 02, gaussian. *Inc., Wallingford, CT* **2009**, *200*.

35. Clyne, M. A.; McDermid, I. S. $B^3\Pi_0$ states of IF, ICI and IBr. Part 1-Calculation of the RKR turning points and Franck-Condon factors for the B-X Systems. *J. Chem. Soc., Faraday Trans. 2* **1976**, *72*, 2242–2251.

36. Clyne, M. A.; McDermid, I. S. $B^3\Pi_0$ states of IF, ICl and IBr. Part 2.-Observation and analysis of the excitation spectra of IF and ICl. *J. Chem. Soc., Faraday Trans. 2* **1976**, *72*, 2252–2268.

37. Takei, T.; Watanabe, A.; Amako, Y. Spectroscopic Constants for the $B^3\Pi_0$ State of $I^{35}Cl$ and for the $B^3\Pi_{0+}$ and B'0^+ States of $I^{37}CI$. *J. Mol. Spectrosc.* **1995**, *171*, 287–290.

38. Rydberg, R. Graphische darstellung einiger bandenspektroskopischer ergebnisse. *Z. Phys.* **1932**, *73*, 376–385.

39. Rydberg, R. Über einige potentialkurven des quecksilberhydrids. *Z. Phys.* **1933**, *80*, 514–524.

40. Klein, O. Zur Berechnung von Potentialkurven für zweiatomige Moleküle mit hilfe von Spektraltermen. *Z. Phys.* **1932**, *76*, 226.

41. Rees, A. The calculation of potential-energy curves from band-spectroscopic data. *Proc. Phys. Soc.* **1947**, *59*, 998.

42. Le Roy, R. J. RKR1: a computer program implementing the first-order RKR method for determining diatomic molecule potential energy functions. *J. Quant. Spectrosc. Radiat. Transfer* **2017**, *186*, 158–166.

43. Le Roy, R. J. LEVEL: A computer program for solving the radial Schrödinger equation

for bound and quasibound levels. *J. Quant. Spectrosc. Radiat. Transfer* **2017**, *186*, 167–178.

44. Western, C. M. PGOPHER: A program for simulating rotational, vibrational and electronic spectra. *J. Quant. Spectrosc. Radiat. Transfer* **2017**, *186*, 221–242.

45. Barker, J. R. Multiple-Well, multiple-path unimolecular reaction systems. I. MultiWell computer program suite. *Int. J. Chem. Kinet.* **2001**, *33*, 232–245.

46. Barker, J.; Nguyen, T.; Stanton, J.; Aieta, C.; Ceotto, M.; Gabas, F.; Kumar, T.; Li, C.; Lohr, L.; Maranzana, A. MultiWell-2017 Software Suite; JR Barker, University of Michigan. *Ann Arbor, Michigan, USA,< year* **2016**,

Graphical TOC Entry

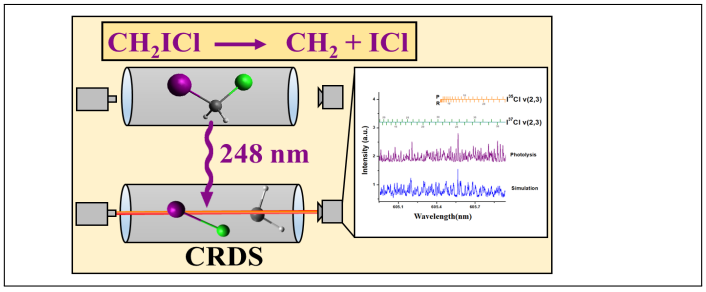

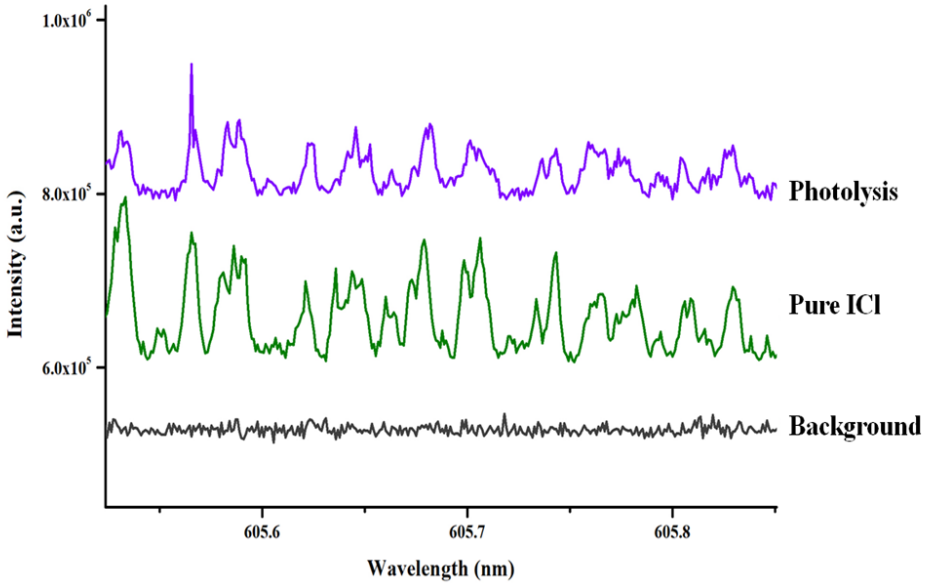

Figure 1: Comparison between a portion of ICl spectra acquired in the photolysis of CH_2ICl at 248 nm) at 0.006 Torr (violet line and pure ICl molecule (green line) and the background spectrum) at 0.034 Torr (grey line).Both spectra are taking at room temperature.

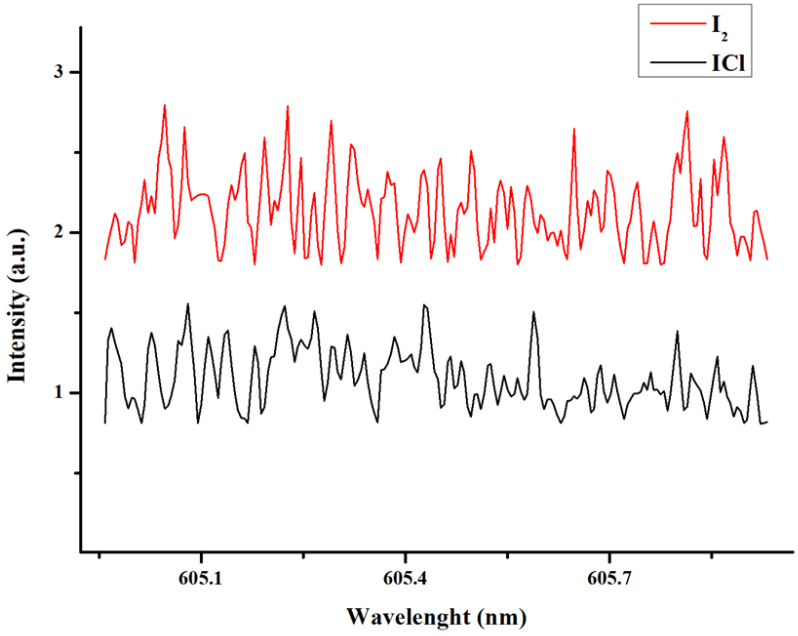

Figure 2: Comparison between a portion of pure ICl spectra) at 0.006 Torr (red line) and pure I_2 molecule at room presure (black line). Both spectra are taking at room temperature.

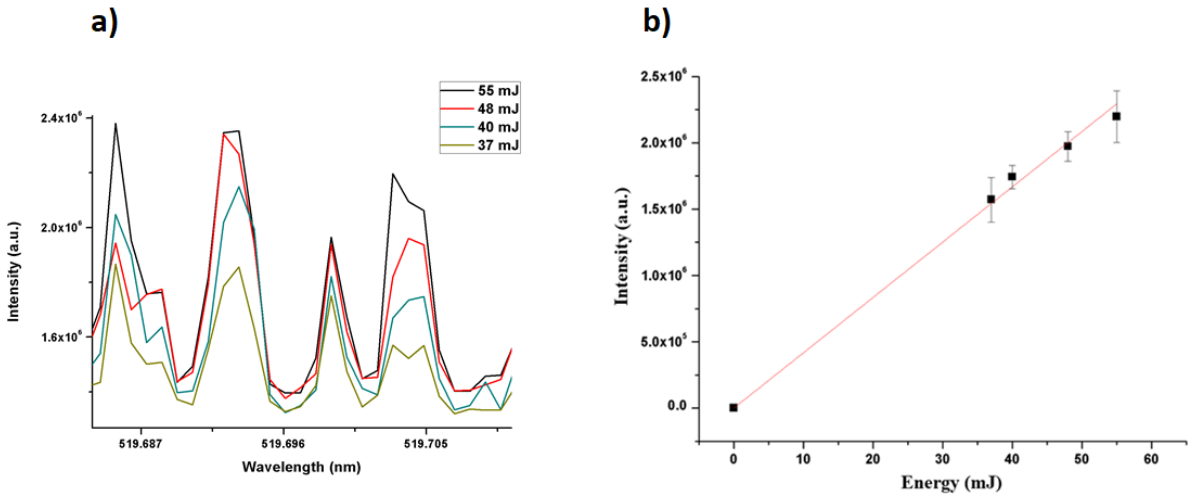

Figure 3: Intensity of ICl fragment as a function of photolysis laser energy varied from 37 to 55 mJ with a pressure of 0.021 Torr at room temperautre. The rotational line at 519.685 nm is selected for this measurement.

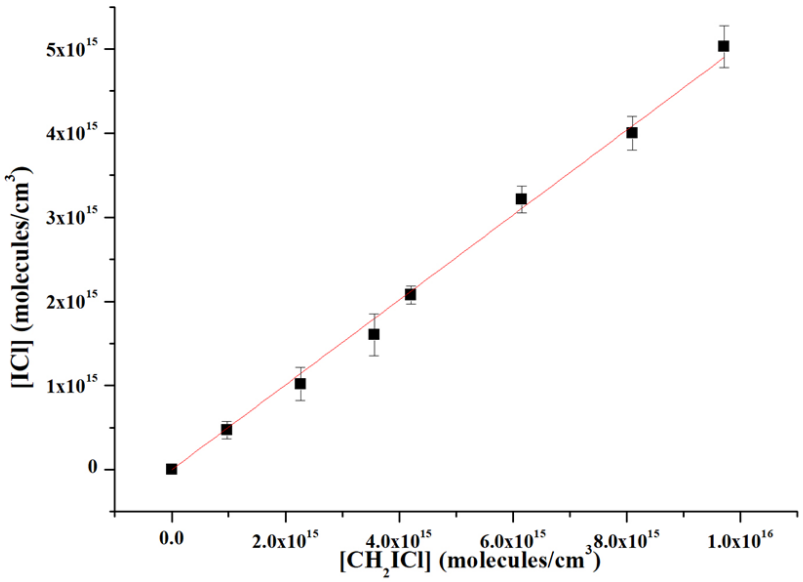

Figure 4: The amount of ICl fragment produced as a function of CH_2ICl concentration varied from 1×10^{15} to 8×10^{15} molecules cm^{-3} at room temperature at 248nm using a laser power of 39 mJ. The rotational line at 519.685 nm is selected for this measurement.

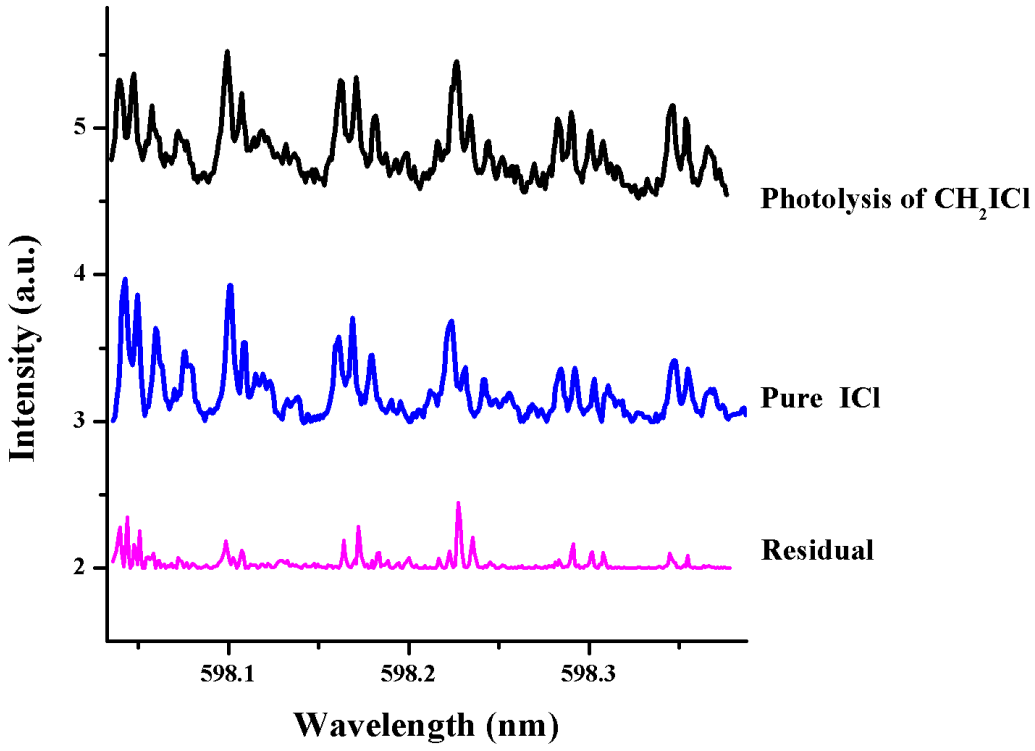

Figure 5: A portion of ICl spectra acquired in the photolysis of CH_2ICl at 248 nm. ICl spectrum from photolysis of CH_2ICl at 248 nm at 0.034 Torr (black line), pure ICl molecule at 0.086 Torr (blue line), and residual spectrum (pink line). Both spectra are taking at room temperature.

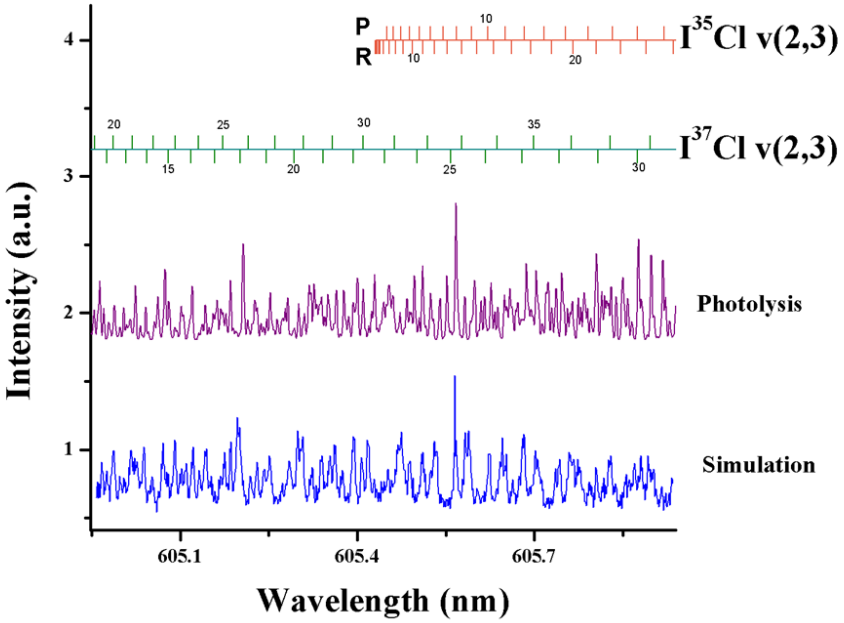

Figure 6: A portion of ICl spectra acquired in the photolysis of CH_2ICl at 248 nm. ICl spectrum from photolysis of CH_2ICl at 248 nm at 0.044 Torr and room temperature(violet line) and simulation of ICl molecule (blue line)

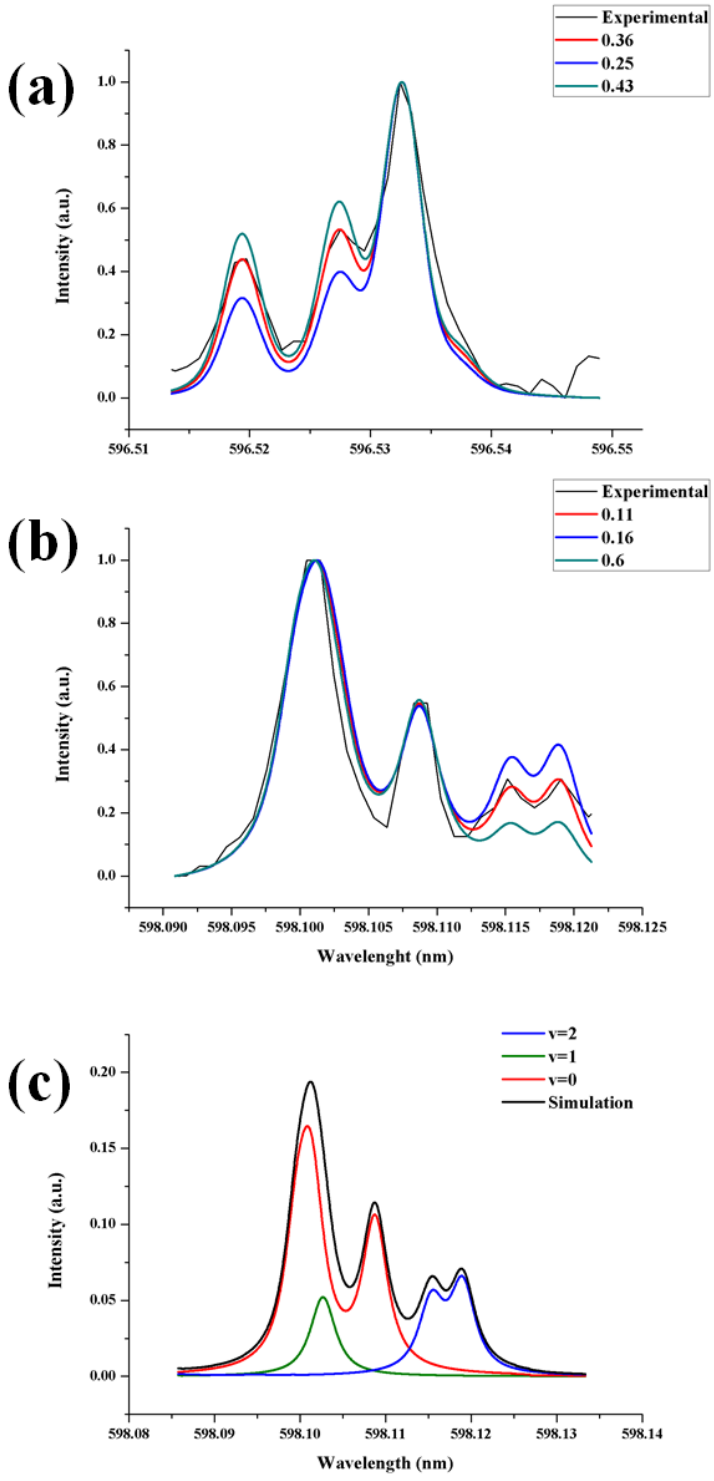

Figure 7: Comparison between experimental and simulated spectra. (a), different population ratio of $(v"=0)/(v"=1)$ fixed at 0.36 at 0.044 Torr. (b) different population ratio of $(v"=0)/(v"=1)$ fixed at 0.36 and $(v"=0)/(v"=2)$ fixed at 0.11 at 0.042 Torr. (c) deconvolution of the simulation with the levels $(v"=0)/(v"=1)$ fixed at 0.36 and $(v"=0)/(v"=2)$ fixed at 0.11. Both spectra are taking at room temperature.

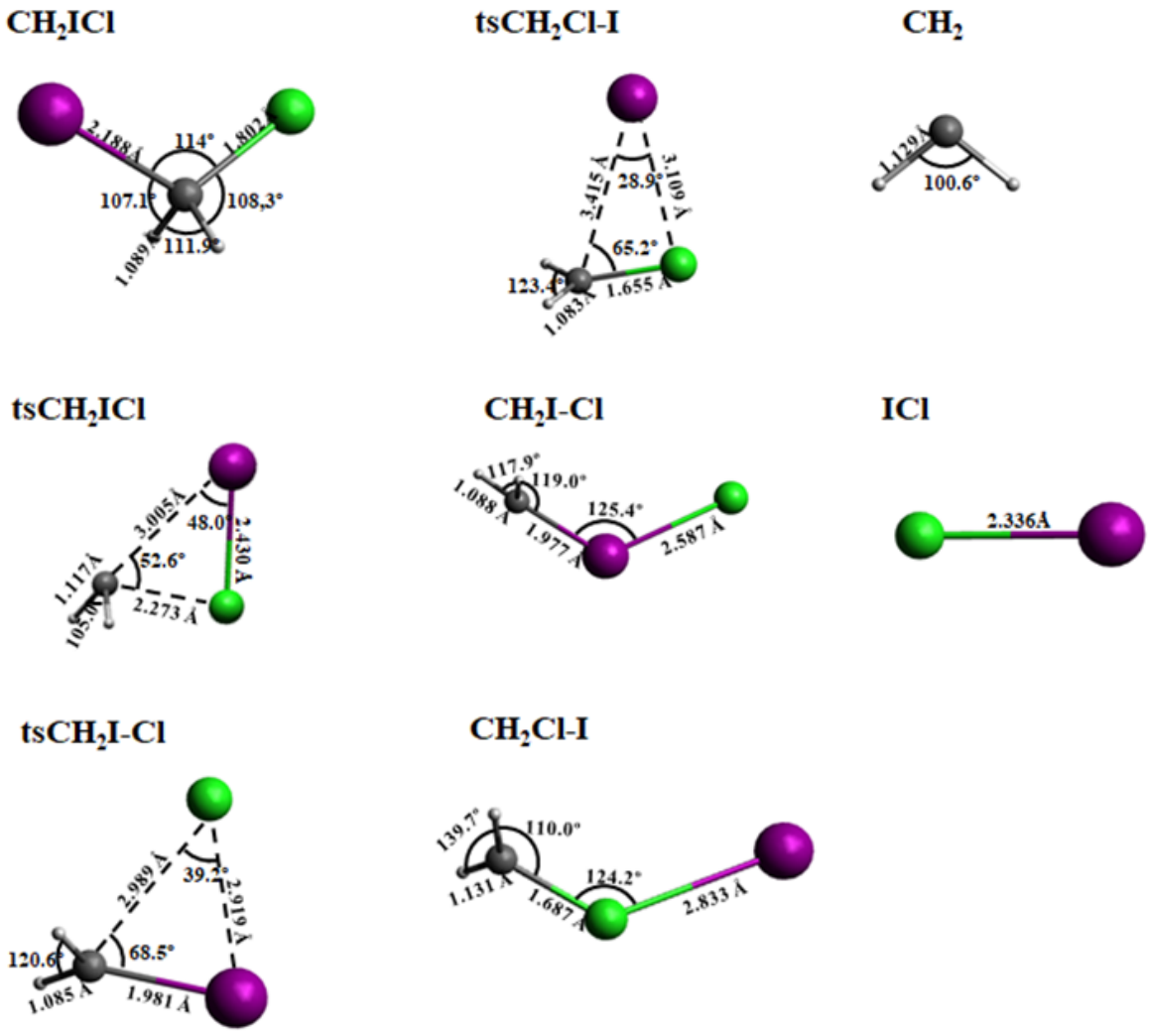

Figure 8: The optimized geometries of reactant, transition state and products for the unimolecular dissociation of CH_2ICl using B3LYP/MIDI! level of theory.

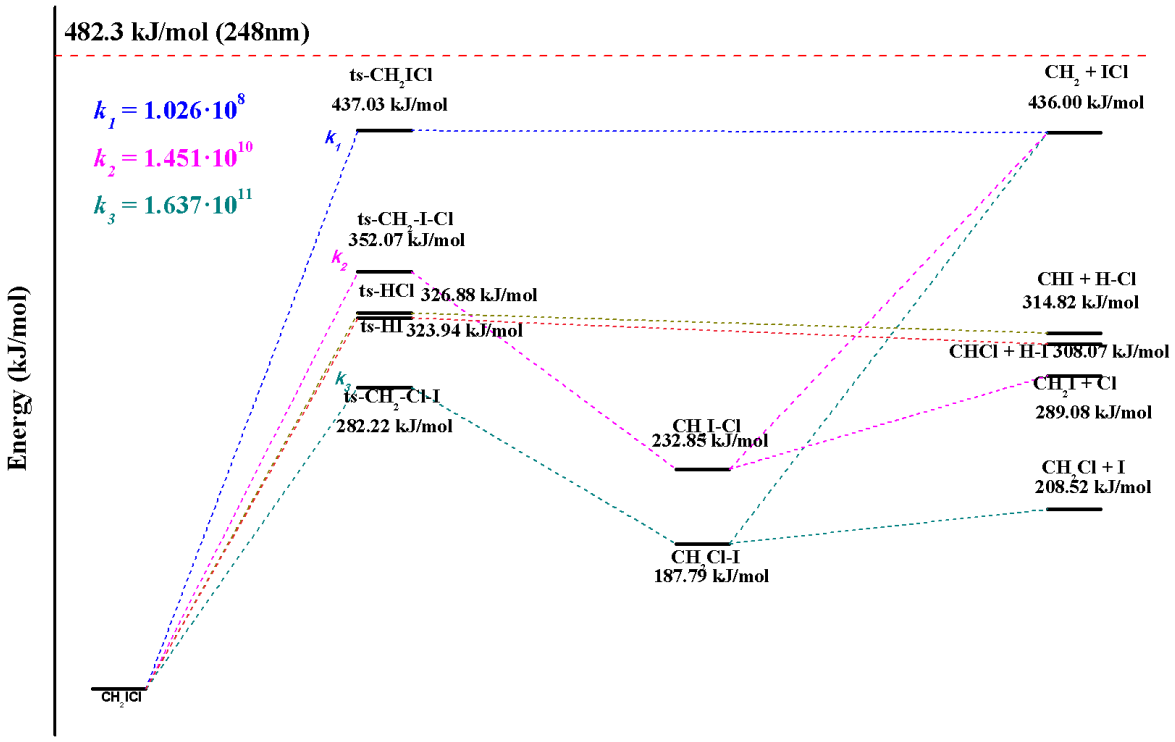

Figure 9: The potential energy surface diagram for the formation of ICl from the CH_2ICl dissociation channel, as computed using CCSD(T)/MIDI! level of theory with B3LYP/MIDI! zero-point energy corrections. The ICl, I, Cl, HCl and HI dissociation channels of CH_2ICl, in which the energies are in kJ/mol relative to CH_2ICl.